# Neutron Transfer to the Ground State of $N^{15}$ in the $N^{14}(N^{14},N^{13})N^{15}$ Reaction*

F. C. Jobes† AND J. A. McIntyre‡

*Physics Department, Yale University, New Haven, Connecticut*

(Received 12 August 1963; revised manuscript received 4 November 1963)

The neutron transfer differential cross sections have been measured at center-of-mass energies of 9, 11, 12, 14, and 16 MeV for the $N^{14}(N^{14},N^{13})N^{15}$ reaction. The energies of the $N^{13}$ nuclei were measured so that the cross sections determined are known to be associated with the transfer of a neutron to the ground state of the residual $N^{15}$ nucleus. It is found (1) that the total cross section for transfer to the ground state of $N^{15}$ is approximately constant over the range of energies studied in contrast to the results of Toth and (2) that a plot of the differential cross section $d\sigma/dR_{min}$ (where $R_{min}$ is the classical distance of closest approach between the nitrogen nuclei) has an exponential dropoff with large $R_{min}$ values that is $\frac{1}{3}$ as steep as that given by the semiclassical tunneling theory of Breit and Ebel at all five energies studied. Finally, by considering recent experimental data taken at reaction energies below the Coulomb barrier where the data do agree with a quantum-mechanical formulation of the tunneling theory, it is argued that the large disagreement between the tunneling theory and the higher energy data presented in this paper can most likely be accounted for by introducing, as Greider has done, a nuclear interaction between the projectile and target nucleus.

## I. INTRODUCTION AND SUMMARY

THE study of neutron transfer reactions is of particular interest because of the information that they would be expected to give about the wave function of the transferred neutron.[1,2] This information can be obtained, however, only if the transfer process takes place via the tunneling mechanism, i.e., the transferred neutron tunnels from the potential well of the projectile into the potential well of the target nucleus. An essential first step, therefore, toward gaining information about the neutron wave function, is to determine experimentally that the transfer of the neutron proceeds by tunneling.

The first calculation of the tunneling mechanism was made by Breit and Ebel[2] who used a semiclassical approximation for the description of the neutron transfer process. While this description was somewhat limited in accuracy, the purpose of its development was to give an orientation to investigators concerning the mechanism involved in the transfer process.

The theory yielded a definite form for the variation of the total cross section for neutron transfer as a function of energy and also predicted a definite function for the differential cross section as a function of the angle for the emitted $N^{13}$ nucleus. The nuclear information, i.e., the magnitude of the neutron wave functions overlapping in the transfer process, appeared in the transfer cross section through a multiplicative co-efficient which determined the magnitude of the transfer cross section.

Comparison of this theory with the experimental data obtained for the $(N^{14},N^{13})$ reactions has been carried out by Breit and Ebel.[2,3] Since the transfer process was usually studied experimentally at energies above the Coulomb barrier, it was clear that care would have to be taken in comparing the experimental data to the tunneling theory. It was found for the total cross section data, that the tunneling theory could be made to fit the data only at the lowest energies where the Coulomb barrier still kept the interacting nuclei apart. For $B^{10}$ and $N^{14}$ large discrepancies still existed however, even at energies considerably below the barrier. A more comprehensive compilation of total cross section data by Toth and Newman[4] has confirmed the uniqueness of $B^{10}$ and $N^{14}$ in this respect, not only for the $(N^{14},N^{13})$ neutron transfer reaction, but also for the $(F^{19},F^{18})$ neutron transfer reaction.[5]

In comparing the semiclassical tunneling theory to angular distributions, Breit and Ebel had available the $N^{14}$ data of Reynolds and Zucker[6] and the $Mg^{25}$ data of Halbert and Zucker.[7] The $Mg^{25}$ data were obtained at an energy well above the Coulomb barrier; nevertheless, because of the semiclassical nature of the nitrogen projectiles, the distant collisions would be expected to be associated with the $N^{13}$ nuclei appearing at small angles. It would not be unreasonable then for the neutron transfer to proceed by tunneling for these particular collisions and, indeed, Breit[3] found that a quali-

* Supported by the U. S. Atomic Energy Commission.

† Present address: Socony Mobil Oil Company, Box 1025, Princeton, New Jersey. This material has been submitted by F. C. Jobes as part of a dissertation for the degree of Doctor of Philosophy at Yale University.

‡ Present address: Texas A&M University, College Station, Texas.

[1] G. Breit, M. H. Hull, and R. L. Gluckstern, Phys. Rev. 87, 74 (1952).

[2] G. Breit and M. E. Ebel, Phys. Rev. 103, 679 (1956). For a discussion of the quantum-mechanical extension, cf. G. Breit, *Handbuch der Physik*, edited by S. Flügge (Springer-Verlag, Berlin, 1959), Vol. 41, Part 1, Sec. 48.

[3] For a comparison of the experimental data with theory see G. Breit, in *Handbuch der Physik*, edited by S. Flügge (Springer-Verlag, Berlin, 1959), Vol. 41, Part 1, Sec. 48; and G. Breit, *Proceedings of the Second Conference on Reactions between Complex Nuclei*, edited by A. Zucker, E. C. Halbert, and F. T. Howard (John Wiley & Sons, Inc., New York, 1960), pp. 1–15.

[4] K. S. Toth and E. Newman, Phys. Rev. 130, 536 (1963).

[5] J. L. Perkin, R. F. Coleman, and D. N. Herbert, Proc. Phys. Soc. (London) 79, 1033 (1962).

[6] H. L. Reynolds and A. Zucker, Phys. Rev. 101, 166 (1956).

[7] M. L. Halbert and A. Zucker, Phys. Rev. 108, 336 (1957).

tative agreement to the tunneling theory was obtained for the $Mg^{25}$ data at the small angles. At the larger angles, corresponding to closer collisions, the experimental data dropped below the tunneling prediction because, as pointed out by Breit, of the absorption of the nitrogen projectiles by the $Mg^{25}$ nuclei. The $Mg^{25}$ angular distribution data therefore appeared to be in harmony with the semiclassical tunneling theory and subsequent, more extensive experimental data on $Au^{197}$ and $Mg^{24}$ confirmed this picture.[8,9]

However, a somewhat different picture was presented by the $(N^{14},N^{13})$ reaction when $N^{14}$ was the target. Here, there were angular distribution data[6] taken at a c.m. energy of 8.2 MeV so that the distance of closest approach between the projectile and the target nucleus was $R=8.6$ F, corresponding to an $r_0$ of over 1.7 F $(r_0=R/(A_1^{1/3}+A_2^{1/3}))$. It seemed reasonable therefore that the tunneling theory would be applicable even for the closest collisions, i.e., for $N^{13}$ nuclei appearing in the back direction. It was found, however, that in the back direction where a comparison between the tunneling theory and experiment could be made, there was a large discrepancy between the experimental angular distributions and the semiclassical tunneling theory.[2,3] Further information on the angular distribution for this reaction was obtained by Toth[10] at 14 MeV and 12 MeV. He found strong disagreement between the tunneling theory and the experimental data even at angles corresponding to very distant collisions $(r_0=7.2$ F). In addition, Toth[11] has shown that the angular distribution from $B^{10}$ also gives a poor fit to the tunneling theory.

The $N^{14}$ and $B^{10}$ nuclei, therefore, have appeared to give anomalous results when their neutron transfer data have been compared to the tunneling theory. In addition, it has been reported for both of these nuclei[10,11] that, as the energy of the bombarding $N^{14}$ nuclei is lowered, the cross section for neutron transfer to the ground state is reduced with respect to transfer to the first excited states of the residual $N^{15}$ and $B^{11}$ nuclei in spite of the unfavorable $Q$ values for such reactions. There seem to be, therefore, important reasons for investigating in more detail the neutron transfer process with these nuclei.

The purpose of this paper is to present the results of further experimental investigation of the $N^{14}(N^{14},N^{13})N^{15}$ reaction in which the transfer of a neutron to the ground state of $N^{15}$ has been isolated from the other transfer processes. (In the simple tunneling process, the detected $N^{13}$ nucleus is always left in its ground state since all of the excited states of $N^{13}$ are proton unstable.) The determination of the nuclear states before and after the transfer process is a necessary step in testing the tunneling theory since the theory applies only for the transfer of the neutron between definite states.

The results of the present investigation can be summarized as follows:

(1) The neutron transfer cross section to the ground state of $N^{15}$ is not reduced at the lower energies $(E_{c.m.}=9$ and 11 MeV) in contradition to Toth's results[10] at 9.9 MeV.

(2) At the higher energies $(E_{c.m.}=12$ and 14 MeV), essential agreement is found between the angular distributions presented here and those previously reported by Toth.[10] The differential cross sections measured here for neutron transfer to the ground state of $N^{15}$ at five different reaction energies are plotted in a semiclassical manner in Fig. 9. In this figure, $d\sigma/dR_{min}$ is plotted against $R_{min}$, where $R_{min}$ is the distance of closest approach between the center of the $N^{14}$ projectile and the $N^{14}$ target nucleus as the projectile moves along a Rutherford scattering trajectory. (The experimental data at the different energies in the figure are normalized to unity at their maximum values.) It is seen that the experimental data at all five energies lie essentially along the same curve when normalized in this manner. For the large $R_{min}$ values the decrease in the experimental $d\sigma/dR_{min}$ values is exponential $(\alpha=0.128$ F$^{-1})$ and is in agreement with the results of Toth[10] at 12 MeV and 14 MeV. However, the peak of the experimental curve appears at an $R_{min}$ value of $8.2\pm0.4$ F, which is a somewhat smaller value than the 10.5 F value reported by Toth.

(3) The differential cross sections for neutron transfer to the ground state of $N^{15}$ at the five different reaction energies $(E_{c.m.}=9, 11, 12, 14,$ and 16 MeV) are all in strong disagreement with the semiclassical approximation[2] of the tunneling theory. The disagreement with the semiclassical tunneling theory is also exhibited in Fig. 9 along with an arbitrarily normalized tunneling theoretical curve, as calculated by Breit and Ebel.[2] The tunneling theory curve clearly cannot be fit at the large values of $R_{min}$ to the experimental curve defined by the letters. (A fit would not be expected for $R_{min}$ values less than 8 F since $N^{13}$ ions on such trajectories will be absorbed by the target nucleus and hence will not emerge from the reaction regardless of the neutron transfer mechanism.)

From the data presented in Fig. 9 it is seen that the discrepancy between theory and experiment at the large $R_{min}$ values is such that, theoretically, the cross section for the transfer of neutrons falls off too fast with increasing $R_{min}$ values. This result is the same as that found by Breit and Ebel[2] in analyzing the data of Reynolds and Zucker.[6] As a result of their analysis, Breit and Ebel at that time suggested[12] that the neutron wave function of the transferred neutron must extend farther from the nucleus than when it was in the ground state (the tunneling theory having used the ground

[8] J. A. McIntyre, T. L. Watts, and F. C. Jobes, Phys. Rev. 119, 1331 (1960).
[9] K. S. Toth, Phys. Rev. 126, 1489 (1962).
[10] K. S. Toth, Phys. Rev. 121, 1190 (1961); 123, 582 (1961).
[11] K. S. Toth, Phys. Rev. 131, 379 (1963).

state extension of the neutron wave function). They therefore looked into the possibility that the neutron was raised to an excited state by the strong Coulomb field of the other nucleus and that the neutron then fell back to the ground state during the transfer process. Their calculations[12] showed that it was indeed possible to produce angular distribution curves of the same qualitative shape as those in Fig. 9. However, the transfer process was no longer such a simple one as the tunneling process.

A different approach for removing the discrepancy in Fig. 9 has recently been proposed by Greider[13] who has calculated the effect of the nuclear interaction on the tunneling process. He has used a $T$-matrix formalism to calculate the tunneling cross section for neutron transfer to the ground state of N$^{15}$ and has attenuated the wave function of the interacting nuclei in the neighborhood of the nuclear interaction region. Comparison is made in his work with the 16-MeV data reported in this paper and is reproduced in Fig. 12. It is seen that the theoretical curve that includes absorption gives a much better fit to the experimental data than either of the tunneling theory curves without absorption. Thus, there are at least two definite possibilities for reconciling the N$^{14}$ data with theory at the large $R_{min}$ values: to introduce a virtual Coulomb excitation process[12] or to take into account the nuclear interaction.[13]

Clearly, as Breit has emphasized, it would be very helpful in understanding the neutron transfer mechanism to carry out experiments at energies below the Coulomb barrier so that nuclear interactions other than the transfer process would not take place to a significant extent. The original concept of tunneling of Breit and his collaborators[1,2] is applicable of course only for energies below the Coulomb barrier. The comparison of the theory to the experiment above the barrier has been carried out only because of the absence of data at the lower energies. Recently, experimental angular distributions for N$^{14}$ target nuclei have been obtained at an energy of 6 MeV (well below the Coulomb barrier energy), and good agreement with the tunneling theory without absorption was found.[14] This agreement between the low energy data and the tunneling theory would then indicate that at the low energy, the contribution from the virtual Coulomb excitation process was small. However, in comparison to tunneling, the virtual Coulomb excitation process is less important at the higher energies.[3] Therefore, the large discrepancy at the higher energies in Fig. 9 between the tunneling theory and the experimental data at the large $R_{min}$ values cannot be accounted for by assuming an im-
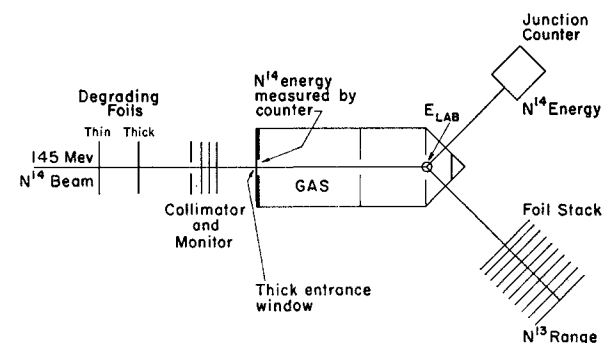


FIG. 1. Schematic drawing of the beam collimation and monitoring system, gas target, foil stack (for detection of N$^{13}$ ions) and junction counter (for detection of elastically scattered N$^{14}$ ions).

portant contribution to the transfer by the virtual Coulomb excitation process. It would appear, that the most likely explanation for the large discrepancy in Fig. 9 between tunneling theory and experiment at the large $R_{min}$ values is that the nuclear interaction modifies the tunneling process as indicated by Greider's curve in Fig. 12. If this conclusion proves to be true, it will be necessary to take into account the nuclear interaction in a careful way if the neutron transfer process is to yield information about neutron wave functions at projectile energies above the Coulomb barrier energy.

The experiments reported in this paper are discussed as follows: A description of the apparatus is given in Sec. II and a discussion of the fundamental measurements of the (N$^{14}$,N$^{13}$) reaction energy, the N$^{13}$ angle, the N$^{14}$ beam intensity, and the reaction cross section follows in Sec. III. The analysis of the experimental data is then considered in Sec. IV and the comparison with theory carried out in Sec. V.

## II. EXPERIMENTAL APPARATUS

The experimental apparatus has been described in detail elsewhere.[15] A schematic diagram of the target holder for the N$^{14}$ gas target, the N$^{13}$ collector foils, and the monitoring devices is given in Fig. 1.

The 145-MeV N$^{14}$ beam from the Yale heavy ion linear accelerator (1% energy resolution) approaches the apparatus from the left in Fig. 1. Two sets of foils, the "thick" set and the "thin" set can be placed in the beam to lower the energy of the N$^{14}$ projectiles by small increments. The beam then passes through a 0.32-cm-diam hole for collimation and through a three-foil beam monitor. The outer two foils of the monitor are held at $+1000$ V potential while the beam intensity reading is taken from the center foil. The reading depends on the number of electrons (delta rays) knocked out of the center foil which are attracted to the outer foils and so has a perfectly linear response to the beam intensity.

After passing through the monitor the beam enters

[12] G. Breit and M. E. Ebel, Phys. Rev. 104, 1030 (1956).

[13] K. R. Greider, Phys. Rev. Letters 9, 392 (1962); K. R. Greider, *Direct Interactions and Nuclear Reaction Mechanisms*, edited by E. Clementel and C. Villi (Gordon and Breach, New York, 1963), p. 971.

[14] L. C. Becker, F. C. Jobes, and J. A. McIntyre, Third Conference on Reactions between Complex Nuclei, Asilomar, April 1963 (unpublished).

[15] J. A. McIntyre, T. L. Watts, and F. C. Jobes, Nucl. Instr. Methods 21, 281 (1963).
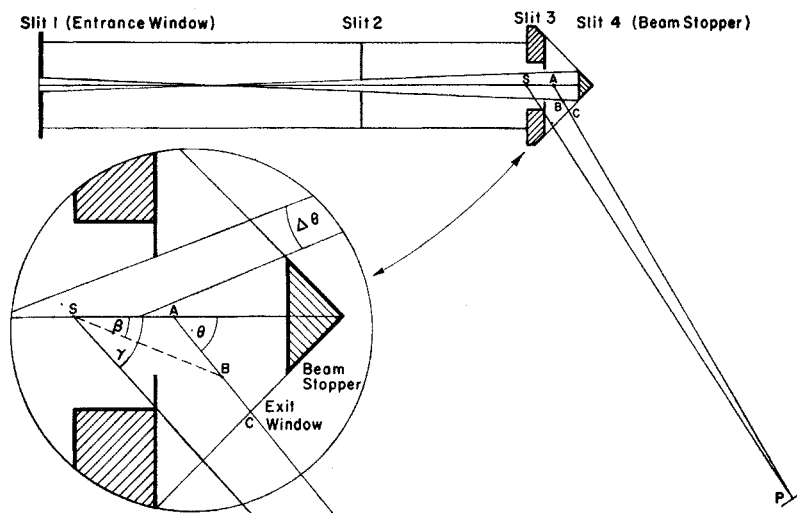
GAS TARGET



FIG. 2. Scale drawing of the target holder for the nitrogen gas target. The enlarged inset shows the geometrical details of the reaction. The center of the 12-in.-diam spherical reaction chamber is at $S$, so that the angular positions inscribed on the inside of the sphere correspond to the angle $\gamma$. The center of the gas volume in which the reaction occurs is at $A$ since ions leaving from this point pass through $B$ which lies halfway between slits 3 and 4. The length of the reaction volume is also determined by the distance between slits 3 and 4; it is the distance between the intersections of the target axis and the lines defining $\Delta\theta$. The angle of emission of the detected $N^{13}$ ion is the angle $\theta$. The length of the target volume, the relation between $\gamma$ and $\theta$, and the location of $A$ are all given in the Appendix.

the target holder by passing through a thick (36.3 mg/cm²) aluminum window. The window is 0.39 cm in diameter so that most of the beam passing through the monitor also passes through the window. Most of the energy loss of the $N^{14}$ projectiles takes place in this window. Further energy loss occurs in the $N^{14}$ gas in the target (pressure=0.35 atm) until the $N^{14}$ projectiles reach the end of the target holder where the beam is stopped. The $N^{13}$ products of the $N^{14}(N^{14},N^{13})N^{15}$ reaction occurring in the active region of the target pass through a ¼ mil (equivalent to 1.12 mg/cm² of aluminum) conical Mylar window and are collected in the foil stack as indicated in Fig. 1. From a measurement of the penetration distance of the $N^{13}$ ions into the foil stack, the energy of the $N^{13}$ ions can be determined. The energy of the $N^{14}$ beam can also be determined by detecting elastically scattered $N^{14}$ ions with a junction counter which is also shown in the Fig. 1.

A cross section of the target holder, drawn to scale, is shown in Fig. 2. The cross section of the $N^{14}$ beam as defined by the tantalum slits inside the holder is also indicated. The region of the gas in the target "viewed" by the collecting foils is bounded at the right by a line from the foils passing through the window at the beam stopper and at the left by a line grazing slit 3. These two boundary lines are shown in the enlarged inset in Fig. 2; they are the lines diverging from the collector foils by the angle $\Delta\theta$. Clearly, the length of gas "viewed" by the collector foils, i.e., the target thickness, is a function of the angle $\theta$.

## III. MEASURING PROCEDURES

### A. Energy Measurements

#### 1. $N^{14}$ Beam Energy

The $N^{14}$ ion beam from the Yale heavy ion linear accelerator has an energy of about 145 MeV. Since the

energies used for the experiments varied between 18 MeV and 32 MeV, the beam energy had to be reduced by a large factor. As mentioned in the last section, the $N^{14}$ beam energy was reduced chiefly by the energy loss of the $N^{14}$ ions passing through the 36.4-mg/cm²-thick entrance window of the target holder. Further energy loss occurred in the 15-cm path through the gas in the target. Adjustment of the energy was obtained by inserting thin foils of aluminum and nickel into the $N^{14}$ beam just before the beam reached the beam collimator (see Fig. 1).

Because the experimental energies of 18 to 32 MeV were so far below the initial $N^{14}$ beam energies particular attention was paid to the determination of the $N^{14}$ energy values used in the experiments. Two independent methods were used to determine $E_{lab}$, the energy of the $N^{14}$ beam at the reaction volume (point $A$ in the inset of Fig. 2) of the target:

(a) The pulse heights from the junction counter (Fig. 1) resulting from $N^{14}$ ions elastically scattered by the nitrogen gas of the target were measured, and

(b) Energy measurements of the incoming $N^{14}$ beam itself were taken. The two methods of measurement gave values for the energy at the reaction volume of the target, $E_{lab}$, agreeing to within 1 MeV of each other.

The two types of measurements were carried out as follows:

(a) The gas scattering measurement was made with the junction counter at a laboratory angle of 20°. The pulse-height calibration of the junction counter was made using the 8.78-MeV and 6.06-MeV alpha particles from $Po^{212}$. The energy of the scattered $N^{14}$ ions striking the counter varied between the values of 7 and 15 MeV, the energy being considerably below the $E_{lab}$ values of 18 to 32 MeV because of energy loss in the gas after scattering as well as in the exit window of the target holder.
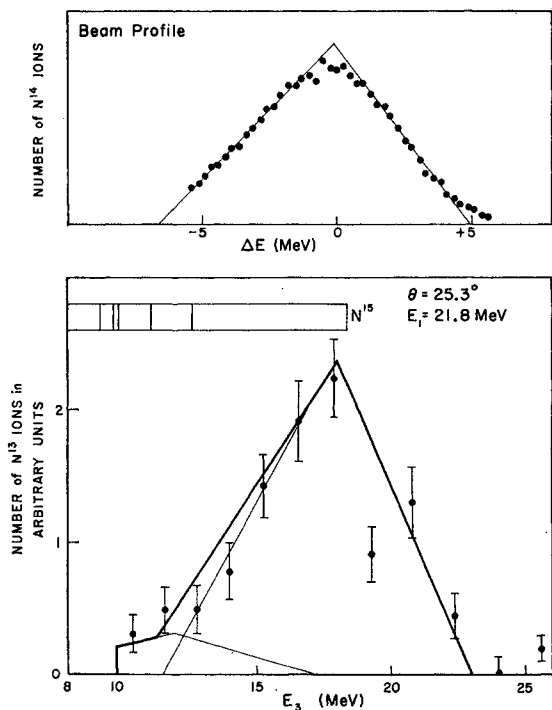
FIG. 3. (a) A pulse-height distribution for elastically scattered N¹⁴ ions obtained with the junction counter. This distribution was considered to be a good representation of the energy profile of the N¹⁴ beam. (b) A plot of the number of N¹³ ions detected in the different foils in the foil stack for a typical (N¹⁴,N¹³) reaction. The ranges of the N¹³ ions, as determined by the positions of the ions in the foil stack, have been converted to energy as discussed in the text. The allowed N¹³ energies, as determined by the excitation of the residual N¹⁵ nucleus, are indicated by the vertical lines at the top of the figure. The experimental data have been fitted using the energy profile of Fig. 3(a) above. The data cutoff at 10 MeV because of the 10 MeV attenuation of the exit window and gas in the targer holder.

($E_{lab}$ is the beam energy at the position of the reaction volume.) The 7- to 15-MeV energy region used was thus near the calibration energy of 8.78 MeV. A pulse-height distribution obtained from the junction counter corresponding to $E_{lab}=32$ MeV is shown in Fig. 3(a). The peak is 5.7 MeV wide at half-maximum with 5 MeV of the width being introduced by the energy spread of the N¹⁴ beam.[16] the rest coming from the 2.7-MeV energy drop across the reaction volume of the gas. (The 5.0- and 2.7-MeV widths when added in quad-

rature give the 5.7-MeV energy spread found experimentally.) Because of the approximate symmetry of the peak in Fig. 3(a) its center can be located to within 0.5 MeV, the peak being quite accurately represented by the triangular shape drawn through the experimental points. Thus, the mean energy of the elastically scattered N¹⁴ ions leaving the target holder was determined to ±0.5 MeV.

The energy loss of the N¹⁴ ions in the Mylar exit window of the target holder was calculated by two methods: (a) the Mylar foil thickness was assumed to be that specified by the manufacturer and its "equivalent aluminum thickness" for stopping N¹⁴ ions was found by dividing by the factor[17] 0.783; (b) the Mylar foil thickness was determined by an alpha-particle gauge[18] with respect to the thickness of a weighed aluminum foil. Both methods yielded a Mylar thickness equivalent to 1.12 mg/cm² of aluminum. The range-energy curves of Northcliffe[19] were then used to determine the energy loss of the N¹⁴ ions in the exit window.

Finally, the energy loss in the gas for the N¹⁴ ions leaving the scattering volume was calculated using the range-energy data of Martin and Northcliffe.[20] The path length in the gas was determined from the geometry of the target as shown in the inset in Fig. 2. Here the distance $AC$ is the mean path length; its formula is given in Eq. (A4) in the Appendix. The mean scattering energy for the N¹⁴ ion beam at point $A$ in Fig. 2 (the center of the reaction volume), was then determined by adding to the junction counter energy the energy loss in the window and in the gas.

(b) The second method for determining the N¹⁴ beam energy at the reaction volume was carried out by removing the target holder from the entrance window and by measuring the beam energy after passing through the entrance window in two ways: (1) by range measurements in aluminum (using the Faraday cup to measure the beam transmission and the secondary beam monitor to monitor the beam) and applying Northcliffe's range-energy relations[19] and (2) by scattering the N¹⁴ beam from a thin bismuth target and measuring the pulse heights of the scattered ions detected by the junction counter. Both methods gave the same value of energy for the N¹⁴ beam that had passed through the entrance window to within 1 MeV. Using the value obtained for the energy of the N¹⁴ beam leaving the entrance window the energy of the N¹⁴ beam at A in Fig. 2 (see inset) was determined by calculating the energy loss of the N¹⁴ ions in the gas in the target holder using the data of Martin and Northcliffe.[20] The

---

[16] This energy spread is not the result of straggling in the energy-degrading material, the straggling being negligible, but rather is the result of the increase in $dE/dx$, the energy loss of the N¹⁴ ion in the stopping material. If $\Delta E_0$ is the energy spread of the high-energy N¹⁴ beam, then $\Delta E$, the energy spread of the degraded-energy beam will be

$$\Delta E = [(dE/dx)_{low}/(dE/dx)_{high}]\Delta E_0, \qquad (1)$$

where the $dE/dx$ values at the high and the low energies are the quantities involved. Since the ratio of $dE/dx$ at different energies is independent of the stopping material for aluminum, plastics, and gases (Refs. 11,13), and is 3.4 for the energies involved (145 MeV and 15 MeV), the initial energy spread of 1% for the 145-MeV N¹⁴ beam, increases to a 5-MeV energy spread at 15 MeV.

[17] P. E. Schambra, A. M. Rauth, and L. C. Northcliffe, Phys. Rev. 120, 1758 (1960).
[18] Of the type described by K. Ramavatorim and D. I. Porat, Nucl. Instr. Methods 1, 239 (1959).
[19] L. C. Northcliffe, Phys. Rev. 120, 1744 (1960).
[20] F. W. Martin and L. C. Northcliffe, Phys. Rev. 128, 1166 (1962).

length of the gas path between the entrance window and $A$ was determined from the geometry of the target holder [see Appendix, Eq. (A3)]. As stated before, the energy of the $N^{14}$ beam at $A$ as determined by this method agreed to within 1 MeV with the energy determined by the detection of $N^{14}$ ions scattered by the nitrogen gas in the target holder. Thus, the $N^{14}$ beam energy at which the $(N^{14},N^{13})$ reaction takes place is considered to be known to $\pm0.5$ MeV, although, as shown in Fig. 3(a) the energy spread of the beam is 5.7 MeV of half-maximum values.

### 2. $N^{13}$ Ion Energy

The energy of the $N^{13}$ ion produced in the $(N^{14},N^{13})$ reaction was determined by a range measurement.[15] Thin ($\sim400$ $\mu g/cm^2$) parlodion foils[21] were stacked at various angles with respect to the $N^{14}$ beam, about half of the azimuthal angle around the beam direction being covered by the foil stacks for each polar angle selected.

The thicknesses of the parlodion foil were measured with the alpha-particle gauge by using as a standard an aluminum foil having a thickness determined by weighing. Each parlodion foil thus was given an "equivalent aluminum thickness" and the aluminum range-energy relations of Northcliffe[19] could be used to determine the $N^{13}$ ion energy loss in the parlodion foils. As a check that the ratio between energy loss in parlodion and aluminum is the same for alpha-particle and nitrogen ions, a stack of parlodion foils was used to degrade the $N^{14}$ beam of the accelerator. It was found that, indeed, the ratio between the energy loss in parlodion and aluminum was the same for $N^{14}$ ions and alpha particles.

The $N^{13}$ range measurements were made by counting, through their radioactive decay, the number of $N^{13}$ ions collected in each foil of the foil stack. The number of $N^{13}$ ions in each foil could then be plotted against the energy of the $N^{13}$ ions striking the foil stack using the energy calibration procedure of the last section to determine the energy of the $N^{13}$ ions entering the foil stack. Inside the foil stack, a $dE/dx$ of 5.0 MeV/mg/cm$^2$ of aluminum was used. The energy of the $N^{13}$ ions leaving the reaction volume of the target could then be obtained by adding in the energy loss of the $N^{13}$ ions in the target gas and in the exit window of the target holder. A plot of the number of $N^{13}$ ions versus the energy of the ions leaving the reaction volume is shown in Fig. 3(b).

Appearing at the top of Fig. 3(b) is an energy level diagram of the $N^{15}$ nucleus. This diagram is adjusted horizontally in such a manner that the ground state line of the $N^{15}$ diagram is located at the $N^{13}$ energy corresponding to an $N^{14}(N^{14},N^{13})N^{15}$ reaction in which

[21] T. L. Watts and C. J. Sneider, Nucl. Instr. Methods 21, 296 (1963).

the $N^{15}$ nucleus is left in its ground state (largest energy possible, then, for the $N^{13}$ ion). The first excited level of the $N^{15}$ diagram is set at the abscissa value corresponding to the $N^{13}$ ion energy resulting from leaving the $N^{15}$ nucleus in its first excited state, etc.

It will be recalled that, in Sec. IIIA1 [see also Fig. 3(a)], the energy of the elastically scattered $N^{14}$ ions leaving the gas target was measured directly with the junction counter to an accuracy of $\pm0.5$ MeV and that this measurement was used to determine the $N^{14}$ beam energy at the reaction volume. It is therefore this energy measurement that is being used to locate the abscissa of the $N^{15}$ energy level diagram in Fig. 3(b). On the other hand, the abscissae of the experimental points in Fig. 3(b) are determined by the range measurements of the $N^{13}$ ions. In *both* determinations an energy loss of the $N^{14}$ and $N^{13}$ ions in the target exit window and in the target gas was introduced so that the energy scale in Fig. 3(b) would be referred back to ion energies at the reaction volume. However, aside from a negligible difference, the energy losses of the $N^{14}$ and $N^{13}$ ions in the target gas and window are identical because of the near equality of the $N^{14}$ and $N^{13}$ ions in their mass, energy, and charge. Therefore, *the relative positions of the abscissa of the experimental points and the $N^{15}$ energy level diagram in Fig. 3(b) are independent of the energy losses assumed in the target gas and window and depend only on the pulse height measurement of the $N^{14}$ ions measured by the junction counter and the range measurement of the $N^{13}$ ions.* Since the energies of the ions occurring in both of these measurements have values between 7 and 15 MeV, an error of at least 40% in either the pulse height or the range measurement would be required to shift the experimental points by 6 MeV from the ground-state position to the first excited state position of the $N^{15}$ level diagram in Fig. 3(b). As already mentioned, the junction counter measurement of the $N^{14}$ ion energy is considered to be accurate to $\pm0.5$ MeV while the thickness values of the approximately 1 MeV-thick parlodion foils are known to an accuracy of at least 5%. The $dE/dx$ value for the energy loss is also known to an accuracy of at least 10%. Thus, the relative position of the $N^{15}$ energy level diagram and the experimental points is known to an accuracy that should easily distinguish transfer reactions to the ground state of $N^{15}$.

A further confirmation of the accuracy of this calibration is furnished by the shape of the peak in Fig. 3(b). If the profile for the peak is assumed to have the same shape as that found for the elastically scattered $N^{14}$ ions in Fig. 3(a), then the $N^{13}$ experimental data can be fitted nicely using a profile centered at the energy corresponding to the ground state of the $N^{15}$ level diagram (the $N^{15}$ nucleus left in its ground state after the $N^{14}(N^{14},N^{13})N^{15}$ reaction); a small contribution must be added from a similar profile centered at the first excited state of the $N^{15}$ diagram.

## B. Angle Measurements

The angles of emission of the N$^{13}$ ions in the (N$^{14}$,N$^{13}$) reaction were determined by scribe lines marked on the inside walls of the spherical reaction chamber. These lines are located by polar and azimuthal angles taken with respect to the geometrical center of the sphere, the polar angles being measured from the line defining the beam direction. Collecting foils were located by their polar angle indicated on the inside of the sphere (denoted by the angle $\gamma$ in Fig. 2). Azimuthal angles did not need to be specified because of the symmetry of the (N$^{14}$,N$^{13}$) reaction about the N$^{14}$ beam axis and the symmetry of the gas target about the same axis.

The actual angle of emission of the N$^{13}$ ions from the reaction, $\theta$, is also shown in Fig. 2 (see inset) and is related to the angle $\gamma$ through a geometrical relation [see Appendix, Eq. (A1)]. Thus, foils placed at a scribe angle $\gamma$, are really at a laboratory angle $\theta$. The laboratory angle $\theta$ is finally transformed to the center-of-mass angle $\theta_{c.m.}$ by the usual transformation.

The angular spread subtended by the collector foils was usually 5°, although for some runs it was half this value. Data were always taken at angles separated by the angular spread used. The beam cross section introduced an angular spread of less than 2°.

## C. Beam Intensity Measurements

The N$^{14}$ ion beam was monitored by measuring the charge collected on the gas target holder. The charge was measured with a Cary electrometer by reading the voltage developed across a standard capacitor. A resistance was placed across the capacitor so that the charge collected would leak away at the same rate as the decay of the radioactive N$^{13}$ ions (10-min half-life). In this way, the charge collected after an interval of beam bombardment would be proportional to the number of N$^{13}$ ions still remaining in the collector foils.

The measurement of the N$^{14}$ ion beam intensity had to be corrected for several factors to yield the desired quantity: the number of N$^{14}$ ions entering the reaction volume of the target, the reaction volume of the target being the region of the target viewed by the N$^{13}$ collecting foils through the Mylar window. The correction factors are the following:

(1) Multiple scattering from the target entrance window reduces the beam magnitude passing through slit 2 below the beam magnitude passing through slit 1 (see Fig. 2).

(2) Electrons knocked out of the outside face of the entrance window can leave the target and hence will increase the target charge collected.

(3) Multiple scattering from the gas in the target will also reduce the beam passing through slit 2.

(4) Some of the beam may not pass through the entrance window but will be stopped in the entrance wall of the target holder.

The following procedure was used to obtain the correction factors for points (1) and (2) above. The secondary beam monitor placed after the beam collimator was read at the same time that the charge collected by the filled target was measured. Next, the target holder was mutilated by removing the beam stopper so that the beam could pass through the target holder and be measured in a Faraday cup. The Faraday cup then measured absolutely the beam passing through the reaction volume of the target. At the same time the secondary beam monitor was read so that it was calibrated in terms of the desired beam quantity. The ratio between secondary beam monitor and target charge collection measured earlier could then be used to calibrate the target charge collection with respect to the Faraday cup reading. This calibration procedure was carried out at each of the N$^{14}$ ion energies used during the experiments.

Since the Faraday cup reading was taken without gas in the target holder, point (3) listed above was not included in the calibration. However, the gas thickness between slits 1 and 2 is only about 4 mg/cm$^2$ compared to the 36 mg/cm$^2$ thickness of the target window and, since the multiple scattering increases in a quadratic manner with increasing thickness of scattering material, the contribution to the multiple scattering by the gas is negligible.

Finally, there is the possibility that the fraction of the 0.32-cm-diam N$^{14}$ ion beam passing through the 0.39-cm-diam target entrance window will not remain constant. The constancy of this factor was not checked directly, but the reproducibility of the reaction cross section data to within 10% for all thirteen measurements but two (the two measurements occurring consecutively after the target holder had been remounted), indicates that the variation in monitor reading from the effect of beam not entering the target was ordinarily less than the 10% value.

However, for the two cases mentioned above, the cross section values increased by 55%. Since the calibration of the monitor with the Faraday cup was carried out after all the cross-section measurements had been taken (and the target holder had been remounted again), an uncertainty of ±50% has been assigned to the absolute calibration of the beam intensity.

## D. N$^{13}$ Yield Measurements

Data were taken in two four-day runs. The beam energy was calibrated before each run as described in Sec. IIIA for the different energies to be studied. In the first run, angular distributions were taken twice at five different energies, 32.0, 26.9, 24.0, 21.2 and 17.4 MeV at the center of the sphere with 5° angular resolution and at the three highest energies with 2.5° resolution. In the second run, angular distribution measurements were made at three different energies, which were at 27.9, 25.0, and 22.2 MeV, or 1 MeV higher than the

three corresponding energies of the first run. Range measurements were also made at 27.9, 22.2, and 18.4 MeV. The calibration of the beam monitor (Sec. IIIC) was performed at the end of the second run.

Background runs were performed at the different energies by filling the target holder with argon gas instead of nitrogen. Because of the high Coulomb barrier of the argon, very little neutron transfer should take place and any $N^{13}$ ions detected would presumably originate from $N^{13}$ ions in the beam scattering from parts of the target or from the argon gas itself. Some background was obtained but this was traced to there being sufficient multiple scattering of the $N^{14}$ beam by the argon gas to cause the beam to hit the outside edges of the beam stopper (see Fig. 2). A calculation showed that this effect would be reduced to less than 10% of the counting rate obtained with nitrogen gas in the target.

For the angular distribution measurements, twelve tapes were placed around the inside of the sphere and, after about 15 min of bombardment, were removed and placed in a positron detection system[22] where the radioactive decay of the collected $N^{13}$ ions was detected. The number of decays was measured each minute for each tape so that the half-life of the decay could be determined. For all cases measured, the half-life was found to be 10 min. For the range measurements a similar procedure was followed for each foil layer in the foil stacks. The efficiency of the positron detection system was measured in the usual fashion.[22]

The results obtained from a typical range measurement are shown in Fig. 3(b), where the number of counts appearing in the different foils in the foil stack is plotted against the $N^{13}$ penetration energy corresponding to the foil. By using the line shape obtained from the elastic scattering of the beam [Fig. 3(a)] and applying this shape at the energies close to the ground state and the first excited state of $N^{15}$ [see Fig. 3(b)], the experimental data could be fitted. Each range curve was fitted in this manner and from these data it was then possible to determine the fraction of the $N^{13}$ ions appearing at a given angle that was associated with the transfer of the neutron to the ground state of $N^{15}$.

## IV. ANALYSIS OF THE DATA

### A. Procedure

A number of steps were required to reduce the experimental angular distributions to a form useful for comparison to theoretical predictions.

(1) Since the experimental angular distributions were obtained by collecting the $N^{13}$ ions on tapes, there was no distinction made between the $N^{13}$ ions corresponding to neutron transfer to the ground state of $N^{15}$ and to neutron transfer to the excited states of $N^{15}$.

[22] F. C. Jobes, J. A. McIntyre, and L. C. Becker, Nucl. Instr. Methods 21, 304 (1963).
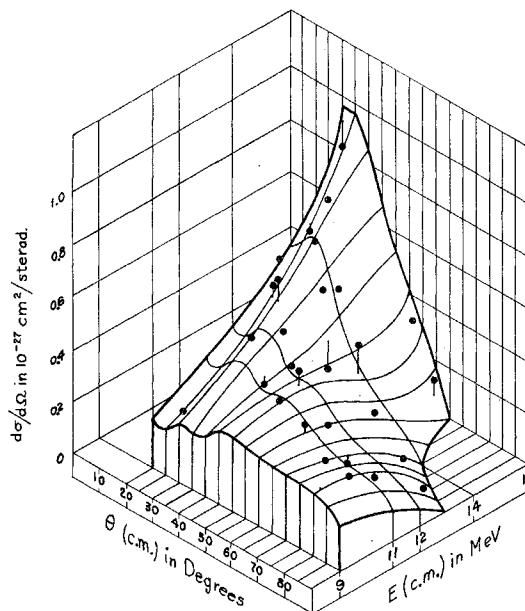
FIG. 4. A plot of $d\sigma(\theta,E)/d\Omega$ against $E$ and $\theta$. The data from the plot are listed in Table I. The surface shown was generated from the experimental points. A number of the points used to generate the surface are not shown since they lie beyond the limits of the plot. The light vertical lines connect experimental points to the surface when the points lie significantly off the surface.

The fraction of the $N^{13}$ ions corresponding to the ground state transfer was therefore obtained from the $N^{13}$ range data such as those shown in Fig. 3(b). The fraction desired is simply the area under the triangle corresponding to ground state transfers divided by the total area under the heavy line. The cutoff at $E_3 = 10$ MeV occurs because $N^{13}$ ions leaving the $(N^{14}, N^{13})$ reaction with energies less than 10 MeV will not escape from the target.

(2) The experimental cross sections $d\sigma/d\Omega$ were then transformed to the center-of-mass system and plotted against the center-of-mass energy of the reaction $E$ and the center-of-mass angle $\theta$ for the direction of the $N^{13}$ ions. This plot of $d\sigma/d\Omega$(c.m.) is shown in Fig. 4, the surface shown being generated by the experimental points. A number of the experimental points used to obtain the surface are not shown in Fig. 4 since they correspond to coordinates of $E$ and $\theta$ beyond the range of those shown in the figure. The deviations of the experimental points from the average surface determined by the totality of the points is indicated by vertical lines which connect the experimental points to the $d\sigma/d\Omega$ surface. Only a few of the points show significant deviations. The deviations have a systematic origin, the statistical error for the points being smaller than the size of the circles representing the experimental values.

(3) For the comparison of the experimental cross sections with theory, it is convenient to express the cross sections $d\sigma/d\Omega$ as a function of $\theta$(c.m.) for a fixed

TABLE I. Summary of the differential cross sections $d\sigma/d\Omega$ (c.m.) in $10^{-27}$ cm²/sr. Errors shown are relative; the absolute value of the cross sections are accurate to ±50%.

### A. For a detector angular spread of ~10° (c.m.)

| $\theta$(c.m.) \ $E$(c.m.) | 9.0 | 11.0 | 12.0 | 14.0 | 16.0 |
|---|---|---|---|---|---|
| 28.0 | 0.220±0.110 | 0.277±0.040 | 0.341±0.034 | 0.590±0.059 | 0.910±0.091 |
| 38.5 | 0.195±0.040 | 0.283±0.040 | 0.342±0.034 | 0.482±0.048 | 0.580±0.058 |
| 49.0 | 0.275±0.055 | 0.308±0.044 | 0.317±0.032 | 0.334±0.033 | 0.325±0.033 |
| 59.5 | 0.253±0.051 | 0.246±0.035 | 0.228±0.023 | 0.143±0.014 | <0.075 |
| 69.9 | 0.242±0.048 | 0.206±0.030 | 0.170±0.017 | <0.027 | |
| 80.4 | 0.241±0.048 | 0.200±0.029 | 0.147±0.015 | | |
| 90.7 | 0.170±0.034 | 0.111±0.016 | 0.063±0.006 | | |

### B. For a detector angular spread of ~5° (c.m.)

| $\theta$(c.m.) \ $E$(c.m.) | 9.0 | 11.0 | 12.0 | 14.0 | 16.0 |
|---|---|---|---|---|---|
| 20.05 | 0.185±0.093 | 0.290±0.058 | 0.370±0.074 | 0.550±0.110 | 0.960±0.192 |
| 25.3 | 0.170±0.085 | 0.290±0.058 | 0.360±0.072 | 0.600±0.120 | 0.960±0.192 |
| 30.7 | 0.225±0.045 | 0.350±0.070 | 0.435±0.087 | 0.650±0.130 | 0.820±0.164 |
| 35.9 | | 0.350±0.070 | 0.400±0.080 | 0.520±0.104 | 0.650±0.130 |
| 41.1 | 0.240±0.120 | 0.280±0.056 | 0.310±0.062 | 0.350±0.070 | 0.490±0.098 |

reaction energy $E$(c.m.). However, the reaction energy $E$ varies with the detection angle $\theta$ for a given bombarding energy because of the change in position of the reaction volume in the gas target (see Fig. 2), this change modifying the energy loss of the beam in the gas of the target holder. Thus a given experimental angular distribution which was taken at one time interval for a given *bombarding energy* corresponds to transfer reactions at different energies for each detection angle $\theta$. It is necessary therefore to obtain the $d\sigma/d\Omega$(c.m.) values for a given *reaction energy* by reading the $d\sigma/d\Omega$(c.m.) values from constant energy slices of the $d\sigma/d\Omega$(c.m.) plot in Fig. 4. The intersections of these slices with the $d\sigma/d\Omega$(c.m.) surface are drawn across the surface. In order to minimize interpolation errors, the $d\sigma/d\Omega$(c.m.) values were obtained for detection angles $\theta$(c.m.) corresponding to experimental angles of detection. These $d\sigma/d\Omega$(c.m.) values are listed in Table I for the five reaction energies $E$(c.m.) of 9, 11, 12, 14, and 16 MeV.

### B. Experimental Errors

As mentioned in the last section, most instances of statistical errors are small. The systematic errors probably arise chiefly from the beam monitoring. Since each angular distribution was obtained during one bombardment, the relative values of the cross sections for each bombarding energy are quite accurate. However, as also discussed in the last section, interpolations are necessary between the cross sections obtained at different bombarding energies if cross sections at a fixed reaction energy are to be obtained. Because of this

requirement, the accuracy of the beam monitoring enters into the determination of even the relative differential cross sections at a fixed reaction energy.

A good estimate of the variation in the beam monitor efficiency could be made by plotting the $d\sigma/d\Omega$ values obtained at a given angle $\theta$ against the eight different bombarding energies $E$. During the first run, angular distributions were taken at each of the five different bombarding energies twice. The two sets of angular distributions agreed with each other to within 10%. Taking the average of the two sets at each angle, smooth curves of $d\sigma/d\Omega$ versus energy were obtained for each detection angle. For the second run, three angular distributions were taken, one fitting in nicely with the data of the first run; the other two however, were 55% high. Since the target holder had been replaced just before these two measurements were made, it has been assumed that the holder was somewhat misaligned so that incorrect monitoring occurred. The angular distributions for these two cases have therefore been reduced by the factor 0.645 to bring them into agreement with the other eleven measurements.

Taking into account the relative monitoring uncertainties, the uncertainties involved in fitting the line shape to the range data, and, for the lowest energy, the statistical uncertainties, the uncertainties in Table I were determined. These uncertainties represent the usual parameter associated with the Gauss error curve. With a few exceptions at the 9-MeV energy, all of the errors indicated lie between 10 and 20%. The absolute values of the cross sections in Table I are less certain however, because of the 55% nonreproducibility found between cross section results measured at different

times. (See Sec. IIIC). This nonreproducibility seemed to be associated with the removal and replacement of the target holder and, since the beam intensity calibration was performed at the end of the run after the target holder had been removed several times for various tests, an uncertainty of $\pm 50\%$ is assigned to the absolute values of the cross sections. This error assignment represents probably the outer limits of uncertainty for a systematic error in the apparatus.

## V. DISCUSSION OF RESULTS

Because of the semiclassical nature of the neutron transfer process it has proved convenient in the past[8] to exhibit the differential cross sections as a plot of $d\sigma/dR_{min}$ versus $R_{min}$. [In this section all parameters are measured in the center-of-mass (c.m.) system.] Here, $R_{min}$ is the distance of closest approach between the $N^{14}$ projectile and the $N^{14}$ target nucleus and is related to the other parameters of the interaction by the expression

$$R_{min}= (ZZ'e^2/2E)(1+\csc^2\theta/2), \qquad (1)$$

where $Z$ and $Z'$ are the atomic number of the projectile and target nucleus, and $E$ and $\theta$ are the center-of-mass reaction energy and angle of emission of the $N^{13}$ ion, respectively. In Sec. A below, the experimental data are presented in $d\sigma/dR_{min}$ plots.

Examination of the $d\sigma/dR_{min}$ plots in Sec. A permits, on the basis of physical arguments, the extrapolation of the differential cross section data to $R_{min}$ values not investigated experimentally. It becomes possible, therefore, to integrate the $d\sigma/dR_{min}$ data over all $R_{min}$ values to obtain the total cross section values at the various reaction energies. This program is carried out in Sec. B below.

The experimental results obtained in Secs. A and B are then compared to other published results in Sec. C, and finally compared to various theoretical predictions in Sec. D.

### A. Transformation to $d\sigma/dR_{min}$

The experimental data $d\sigma/d\Omega$ in Table I are transformed to $d\sigma/dR_{min}$ using the relationship

$$d\sigma/dR_{min}= - (16\pi E/ZZ'e^2) \sin^3(\theta/2)d\sigma/d\Omega. \qquad (2)$$

This relationship follows immediately[8] from the relation between $R_{min}$ and $\theta$ given in Eq. (1). Plots of $d\sigma/dR_{min}$ versus $R_{min}$ are given in Fig. 5 for the five different reaction energies (the different curves are multiplied by different powers of 10 for display purposes).

All of the $d\sigma/dR_{min}$ plots show a similar form in contrast to the $d\sigma/d\Omega$ plots in Fig. 4. At large $R_{min}$ values the cross section drops exponentially with increasing $R_{min}$. For the smallest $R_{min}$ values, the cross section is seen to drop abruptly from a peak value occurring near $R_{min}=8$ F. This behavior is typical for
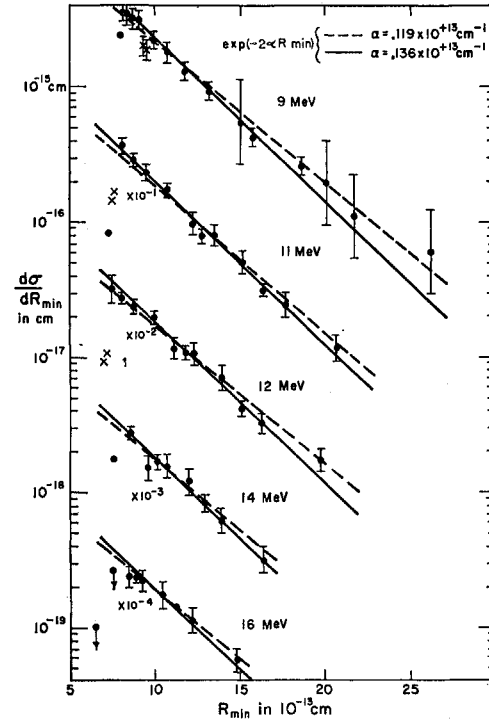
FIG. 5. Plots of the differential cross section $d\sigma/dR_{min}$ for the five different reaction energies studied. The two exponential curves on each plot indicate the range of $\alpha$ that can be used to fit the data if a function of the form $\exp(-2\alpha R_{min})$ is assumed.

neutron transfer reactions and can be explained in semiclassical terms.[8] For large $R_{min}$ values, the projectile and target nuclei do not "touch" and the neutron must tunnel from the potential well of the projectile nucleus to the potential well of the target nucleus. The probability for tunneling increases as $R_{min}$ decreases until at an $R_{min}$ value of about 8 F the nuclei come into "contact." For smaller $R_{min}$ values the $N^{14}$ projectile must penetrate part of the target nucleus and consequently the number of $N^{13}$ nuclei escaping from the collision drops off rapidly.

A complication is introduced into this simple picture however, because of the identity of the projectile and target nuclei in this experiment. At a given detection angle in the forward direction, $N^{13}$ ions can appear either from a small-angle distant collision (here the direct particle or projectile is detected) or from a large-angle close collision (where the recoil particle is detected). These two possibilities are indicated schematically in Fig. 6. However, there is no way in the detection process to distinguish between the two possibilities and so the scattering amplitudes of the two types of scattering must be added rather than the two cross sections. Thus, interference or cross terms will appear in the cross section and a semiclassical transformation to $d\sigma/dR_{min}$ cannot be made.

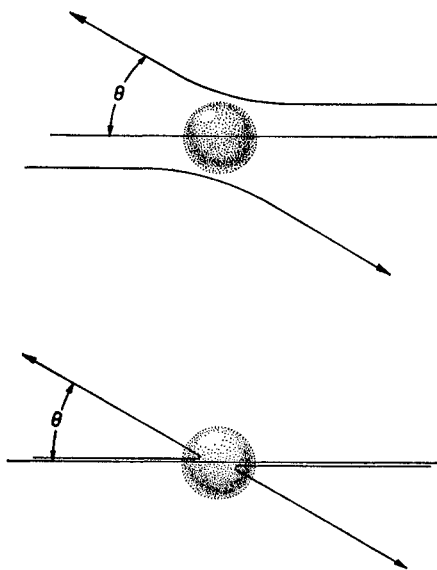This difficulty does not apply however in the high energy (12, 14 and 16 MeV) cases because of the ab-

FIG. 6. A schematic drawing showing classical trajectories for distant and close collisions which each produce a N¹³ ion at the same angle $\theta$. The spherical region at the center represents the region where the nuclear interaction is large.

sorption of the particles in the close-collision case. (See Fig. 6.) Thus, only the direct particles will emerge from the reaction and no interference can take place. This situation is depicted in the top drawing in Fig. 7 where schematic angular distributions are shown. At
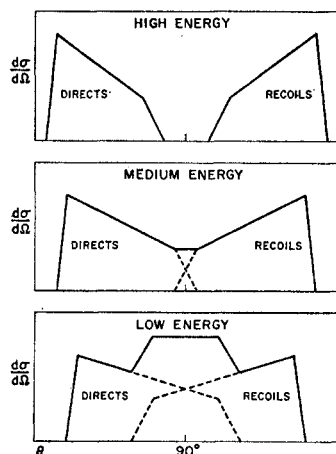


FIG. 7. Schematic diagrams showing the angular regions covered by the N¹³ ions resulting from projectile nuclei (directs) and the N¹³ ions resulting from target nuclei (recoils). The shape of the curves is fairly realistic. In the upper left curve, for example, the sharp rise at the left corresponds to the sharp increase in cross section occurring when the N¹⁴ projectiles come closer to the target nucleus. The drop to the right of the peak reflects the decrease in $d\sigma/d\Omega$ due to the decrease in $dR_{min}/d\Omega$ as $\theta$ increases. Finally, the distribution breaks away from this slope and drops to zero due to nuclear absorption at the large $\theta$ (small $R_{min}$ values). As the projectile energy is lowered, (see lower figures) the "direct" ions move to larger angles while the "recoil" ions (whose distribution in angle is a reflection about 90° of the direct distribution) move to smaller angles. Quantum mechanical interference will occur where the distributions overlap.

the larger angles (corresponding to the smaller $R_{min}$ values) there are no direct particles while at the smaller angles there are no recoil particles. Thus, there are no angles at which both direct and recoil particles emerge. However, as the energy of the reaction is reduced, the projectile is deflected to a larger angle for the same $R_{min}$ value so that the angular region for the direct particles moves to the larger angles while the recoil particles appear at smaller angles. Overlap between the direct and recoil regions therefore occurs at the lower energies as is shown schematically in the two lower diagrams of Fig. 7.
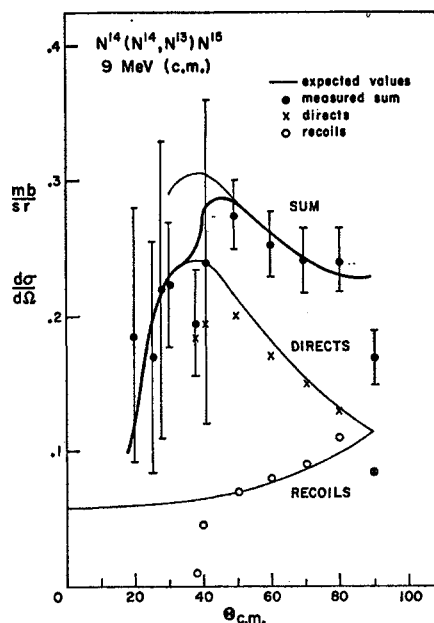


FIG. 8. A plot of the angular distribution obtained at 9 MeV. The experimental points have been considered to be produced by the sum of direct and recoil ions, the direct contribution being indicated by the × symbol, the recoil contribution by the o symbol. The "direct" points correspond to large $R_{min}$ values and the "recoil" points to small $R_{min}$ values, these data being really only a re-plot of the points in the top curve of Fig. 5. A mean exponential curve fitting the data in Fig. 5 is plotted as the light curve in Fig. 8. The cutoff at small $R_{min}$ values in Fig. 5 manifests itself as the cutoff for the "recoils" at 40° in Fig. 8. The heavy line in Fig. 8 corresponds to the sum of the two light lines for angles greater than 40°; for angles less than 40° the contribution of the bottom line is omitted and the heavy line drops to the "directs" line. The magnitude of the point at 90° is seen to be about $\frac{2}{3}$ that of the neighboring angles. This fact is in agreement with the prediction of Breit and Ebel (Ref. 2) and is due to the quantum-mechanical interference between the amplitudes of the "direct" and "recoil" waves.

It was therefore necessary in transforming the 11-MeV and 9-MeV $d\sigma/d\Omega$ data to $d\sigma/dR_{min}$ plots, to divide the $d\sigma/d\Omega$ cross section in a "direct" part and a "recoil" part. The procedure used at 9 MeV is illustrated in Fig. 8. The experimental data are shown; also shown is the contribution to the data of the "direct" particles and the "recoil" particles. Clearly, this division of the experimental data into a "direct"
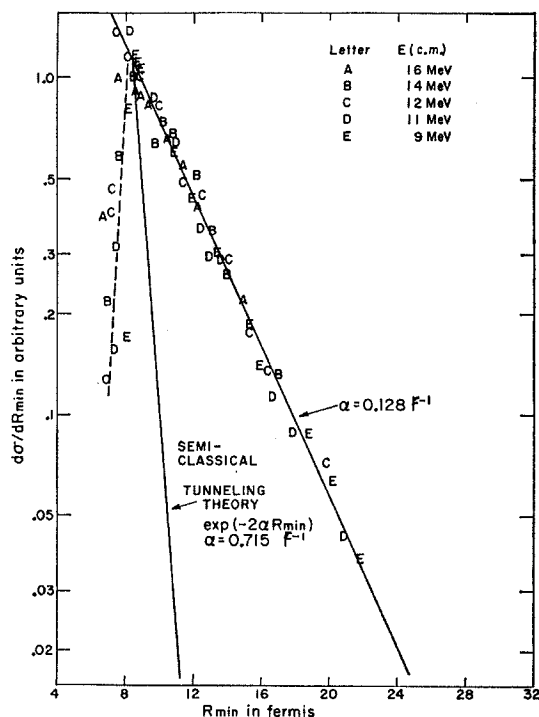
FIG. 9. A plot combining the experimental differential cross section data taken at all five energies: 9, 11, 12, 14, and 16 MeV. The letters each correspond to a different center-of-mass energy as indicated and represent experimental points. The data are the same as those plotted in Fig. 5 except that the data at the different energies have been arbitrarily normalized with respect to one another. Also shown in the figure is the prediction of the Breit-Ebel semiclassical approximation of the tunneling theory which has also been arbitrarily normalized.

and "recoil" component is not only an arbitrary one but also ignores the interference effects between the direct and recoil particles. However, Breit[23] has shown that the spacing of the points in Fig. 8 is large enough to miss the oscillatory features of the interference effects except for the 90° point which should be reduced to $\frac{2}{3}$ of the average value (this reduction is evident in Fig. 8). The division in Fig. 8 was made in such a way that the $d\sigma/dR_{min}$ plot for the 9-MeV data in Fig. 5 yielded a curve similar to the curves at the higher energies. Other divisions of the data in Fig. 8 were tried but all yielded strange curves with inflections. It is felt therefore that the division shown in Fig. 8 is the correct one. These remarks apply also to the 11-MeV data in Fig. 5 which, however, contain less overlap of the direct and recoil regions.

The experimental curves in Fig. 5 have all been fitted with two exponential curves which give an upper and lower limit to the exponential fit. A curve combining all of the experimental results is shown in Fig. 9; the experimental data at the different energies being

normalized to unity at their maximum values. The letters indicate experimental points, a different letter being assigned to each value for the reaction energy. It is seen that the experimental data at the different energies all lie on one curve, this curve giving the differential cross section for the direct particle only. The experimental curve on the large $R_{min}$ side of the peak can be fit quite well[24] with an exponential function $e^{-2\alpha R_{min}}$, where $\alpha = 0.128$ F$^{-1}$.

## B. Total Cross Sections

Inspection of Fig. 9 shows that the largest part of the differential cross section $d\sigma/dR_{min}$ has been measured and that a reasonable extrapolation of the curves to $R_{min} = 0$ and $R_{min} - \infty$ should yield quite accurate values for the total cross sections. When this procedure is followed and $\sigma = 2\int_0^\infty (d\sigma/dR_{min})dR_{min}$ is calculated (the factor of 2 arising from the counting of both the direct and the recoil particles), the results shown in Fig. 10 are obtained. It should be remembered that the absolute values of these cross sections are accurate only to ±50% (see Sec. IVB), while the accuracy of the relative values are indicated by the error bars on the points. It is seen that the total cross section for neutron transfer to the ground state of N$^{15}$ is essentially constant over the range of energies studied in these experiments.

## C. Comparison of Results to Other Data

Also plotted in Fig. 10 are the total cross section values obtained by Reynolds and Zucker[6] for the N$^{14}$(N$^{14}$,N$^{13}$)N$^{15}$ reaction, the final state of the N$^{15}$
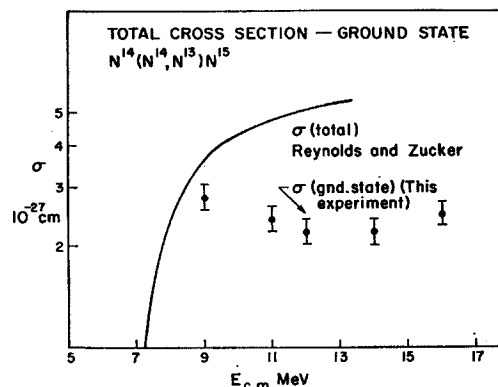


FIG. 10. A plot of the total cross section data for neutron transfer to the ground state of N$^{15}$. Also plotted are the results of Reynolds and Zucker (Ref. 4) who measured the total cross section for neutron transfer to all the energy levels of N$^{15}$. The ordinate scale for the experimental points is accurate to only ±50%. However, the accuracy of the experimental points relative to one another is much less, being indicated by the error bars on the points.

---

[23] G. Breit, *Direct Interactions and Nuclear Reaction Mechanisms*, edited by E. Clementel and C. Villi (Gordon and Breach, New York, 1963), p. 480.

[24] In a preliminary report of these results [Bull. Am. Phys. Soc. **7**, 337 (1962)], the experimental data were said to be fit by an expression of the form $e^{-\alpha r} + e^{-\beta r}$. A more careful analysis of the geometry of the gas target has modified the data to the form presented here.
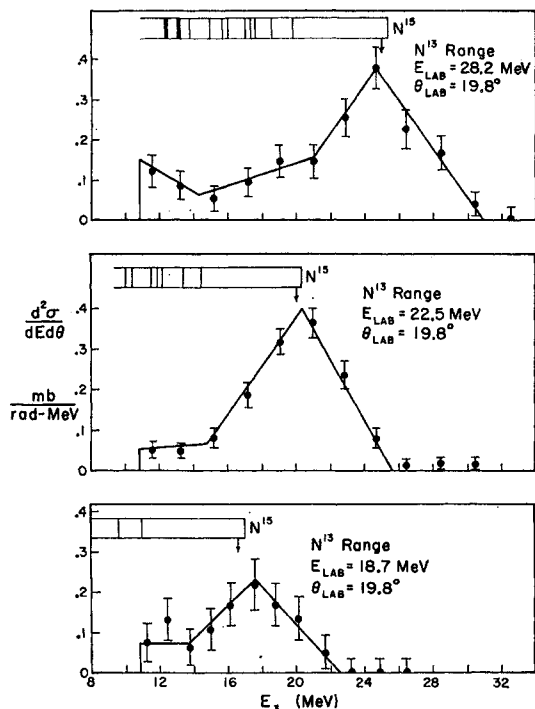
FIG. 11. Energy data for the N¹³ ions leaving the (N¹⁴,N¹³) reaction as determined from range measurements. Data taken at three different bombarding energies are shown. The allowed N¹³ energies, as determined by the excitations of the residual N¹⁵ nucleus, are indicated by the vertical lines at the top of each drawing. The vertical arrow below the N¹⁵ scale indicates the energy at which elastically scattered N¹⁴ ions appeared, the energy being measured with a junction counter. The junction counter energy measurement was used in this way to determine the location of the N¹⁵ energy level scale with respect to the abscissa. The line shapes fitted to the experimental data are determined in the same way as the fit obtained in Fig. 3(b).

nucleus being unknown (in fact, the neutron might not even be bound to the N¹⁵ nucleus). Their cross section values are larger than ours, the difference between the results arising from the contribution of neutron transfers to excited states of N¹⁵. Because of the ±50% uncertainty in our normalization, however, not much information about the magnitude of the transfer to excited states of N¹⁵ can be deduced from the data in Fig. 10.

Comparison of the data can also be made with the measurements of Toth[10] who has studied neutron transfer to the ground state of N¹⁵. While he found transfer to the ground state at the higher energies he reports no transfer to the ground state at 9.9 MeV, which disagrees with the results reported here. Because of these earlier data of Toth's, a careful check was made in these experiments on the energy of the N¹³ ions leaving the reaction (see Sec. IIIA). Typical N¹³ range (energy) data for several reaction energies are shown in Fig. 11. In all, forty range measurements of this kind were made. For each energy studied, the energy of a large fraction of the N¹³ ions corresponded clearly with

neutron transfer to the ground state of N¹⁵. The arrow in each drawing corresponds to the energy of the elastically scattered N¹⁴ ions which were used to locate the N¹⁵ energy level diagram on the drawing. It is very difficult, particularly for the low energy data in the bottom drawing, to understand how an error in range calibration could be made that would be sufficiently large to shift the peak from the energy corresponding to the first excited state of N¹⁵ to the 6 MeV higher energy corresponding to the ground state. In particular, since 11 MeV of energy is lost in leaving the target (see Fig. 11) both the N¹³ and the elastically scattered N¹⁴ ions have only 7 MeV of energy after leaving the target. It would be almost impossible to not be able to determine whether the N¹³ energy were 7 MeV, corresponding to N¹⁵ ground state transfer, or 1 MeV, corresponding to N¹⁵ excited state transfer. We therefore feel that a significant fraction[25] of the neutrons transferred at 9 MeV do go to the ground state of N¹⁵.

## D. Comparison of Experimental Results to Theory

As emphasized in the Introduction, the chief motivation behind the experimental study of the neutron transfer reaction is to obtain information about the magnitude of the transferred neutron wave function at the surface of the nucleus. However, before this desired information can be obtained, the validity of the tunneling theory for describing the neutron transfer process must be demonstrated. As pointed out in the Introduction, the semiclassical tunneling theory predicts a certain behavior for $\sigma(E)$, the variation of the total transfer cross section with energy, and a certain behavior for $d\sigma(\theta)/d\Omega$, the variation of the differential cross sections with angle. These predictions of the tunneling theory will now be compared to the experimental results.

A complication immediately arises when comparison to experimental results is attempted. The tunneling theory, and indeed, the whole concept of a neutron tunneling from the internal field of the projectile to the target nucleus, breaks down once the projectile and the target nucleus come into contact. Thus, the experimental data can only be compared to the tunneling theory for situations where such contact does not occur.

For a comparison of the total cross section data with the tunneling theory, the requirement of no contact applies for all trajectories for the projectile; thus the energy of the projectile must be well below the Coulomb barrier energy of approximately 8 MeV. The total cross section data presented in this paper which

²⁵ It might be argued that these data are not in disagreement with Toth's since the high energy N¹⁴ ions in the 5.7-MeV-wide N¹⁴ beam account for the ground state transfers found at a mean energy of 9 MeV. If it were true that only the high energy tail of the beam were producing the ground state transfers at 9 MeV then the cross section for such transfers should drop a significant amount. Such a drop does not occur, however (see Fig. 10).

were obtained for energies of 9 MeV and greater can therefore not be compared to the tunneling theory.

However, the differential cross section data, $d\sigma/dR_{\min}$, can presumably be compared to the tunneling theory for $R_{\min}$ values greater than the nuclear interaction radius of about 8 F. The fact that a realistic comparison can be made for some values of $R_{\min}$ depends on the accuracy of the semiclassical idea that the nitrogen projectiles follow reasonably well-defined trajectories in passing the strongly absorbing target nuclei.

The tunneling theory as calculated with the semiclassical approximation[2] has therefore been compared to the experimental data in Fig. 9 for the large $R_{\min}$ values. The tunneling curve has been arbitrarily normalized. (Actually, its normalization is energy-dependent although the slope does not change with the reaction energy.) Clearly, the tunneling theory gives a very poor fit to the experimental data even at the largest $R_{\min}$ values. Quantitatively, the experimental curve, $e^{-2\alpha R_{\min}}$, has a value[24] of 0.128 $F^{-1}$ for $\alpha$, while the semiclassically calculated tunneling curve $e^{-2\alpha R_{\min}}$ has a value[26] of 0.715 $F^{-1}$ for $\alpha$. The experimental and theoretical values for $\alpha$ thus differ by more than a factor of 5.

As already discussed in the Introduction, a much better description of the experimental data can be achieved either by postulating a virtual Coulomb excitation of the transferred neutron[12] or by introducing the effect of the nuclear interaction into the $T$-matrix tunneling theory.[13] A comparison by Greider[13] of the 16-MeV experimental data with the tunneling theory modified by the effect of the nuclear interaction is shown in Fig. 12. The nuclear interaction was introduced by an absorption model which attenuates the wave function of the two nuclei inside an interaction volume. The half-value of the attenuation occurs at 7.2 F, corresponding to an $r_0$ of 1.5 F. The attenuation rises from zero to complete attenuation over a radial distance comparable to that found for the nuclear surface thickness from electron scattering measurements[27] (5 F from 10% to 90% absorption). Also shown in Fig. 12 are curves for the tunneling theory in which nuclear absorption has been ignored. One of these curves was calculated using the $T$-matrix formalism,[13] the method used to introduce nuclear absorption into the calculation; the other curve was calculated using the semiclassical method.[2] Qualitatively, the curves are seen to be similar. Clearly, the introduction of nuclear absorption improves the fit to the data even for $R_{\min}$
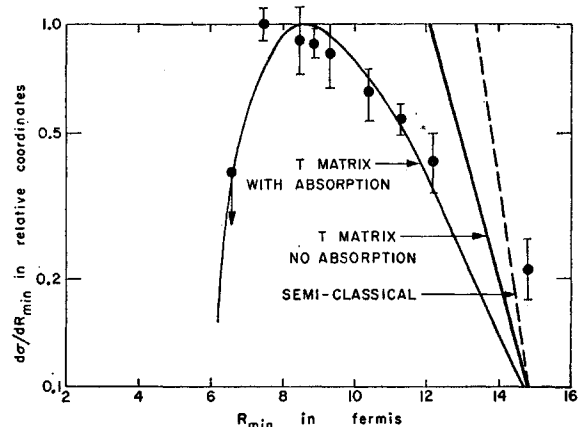


FIG. 12. A comparison of the 16-MeV experimental data to various tunneling theory calculations. The $T$-matrix theory of Greider with and without nuclear absorption is shown (taken from Ref. 9) along with the semiclassical theory of Breit and Ebel (Ref. 2) without absorption. The $T$-matrix and semiclassical curves have been independently normalized.

values much larger than the absorption radius of 7.2 F.

As discussed in the Introduction, later measurements[14] at 6 MeV show that the tunneling theory without absorption does fit the angular distribution data quite well at this lower energy (when arbitrarily normalized). Thus, it seems likely that the virtually Coulomb excitation process contributes at most a small amount to the neutron transfer at this lower energy, and presumably an even smaller amount[3] at the higher energies which were studied in this paper. It would appear then, that the most likely explanation for the large discrepancy between the semiclassical tunneling theory and the experimental data in Fig. 9 is the absence of the nuclear interaction in the formulation of the theory.

## ACKNOWLEDGMENTS

## APPENDIX

Collected here are some of the geometrical relationships related to the scattering process inside the target holder. The symbols used are defined in Fig. 2.

The relationship between the scattering angle $\theta$ and the angle measured from the center of the sphere $\gamma$

---

[26] A more precise expression for the tunneling curve would be the one suggested by Breit (Ref. 2), where $\exp(-2\alpha R_{\min})$ is replaced by $\exp(-\alpha R_{\min}-\bar{\alpha}\bar{R}_{\min})$, $\bar{\alpha}$ and $\bar{R}_{\min}$ being the values of $\alpha$ and $R_{\min}$ corresponding to the neutron binding energy and the separation of the two nuclei, respectively, after the transfer of the neutron. For the reaction under study there is only a difference of a few percent in the value of the exponential value used $[\exp(-2\alpha R_{\min})]$ and the more accurate expression given in this footnote.

[27] See, e.g., R. Hofstadter, Rev. Mod. Phys. 28, 214 (1956).

(the scribe lines on the inside of the spherical reaction chamber are determined by this angle $\gamma$), may be expressed as

$$\sin(\gamma-\theta) = \frac{(B/R)\sin(\beta-\gamma)}{[1+(B/R)^2-2(B/R)\cos(\beta-\gamma)]^{1/2}}. \quad (A1)$$

Here $B$ is the distance from the sphere center to the point half-way between slit edges (line $BS$), $R$ is the radius of the sphere, and $\beta=21.75°$ is the polar angle of the line $BS$. For the target dimensions used, the denominator varied about $1/2\%$ for $0<\gamma<90°$, so that the following relationship was used for the calculations in this paper:

$$\sin(\gamma-\theta)=0.0892\sin(\beta-\gamma). \quad (A2)$$

The location of the center of the reaction volume can be found by using the following expression for the length $AS$:

$$AS=B\sin(\beta-\gamma)/[\sin\gamma-(B/R)\sin\beta]. \quad (A3)$$

The path length of the N¹³ ion leaving the target holder is equal to the distance $AC$ where

$$AC=B\sin\beta/\sin\theta+(W/2)\sin\alpha/\sin(\theta+\alpha), \quad (A4)$$

$W$ being the slit width, i.e., the distance between slit 3 and slit 4, and $\alpha=45°$ being the angle between the exit window and the beam axis.

The path length $l$ of the N¹³ when passing through the window is, simply,

$$l=\tau/\sin(\theta+45°), \quad (A5)$$

where $\tau$ is the window thickness.

Finally, the length $L$ of the reaction volume along the beam axis is

$$L=W\sin\gamma/[\sin\gamma-(B/R)\sin\beta]. \quad (A6)$$

# Cross Sections for the Ni⁵⁸(α,p), Ni⁵⁸(α,γ), and Co⁵⁹(α,n) Reactions

F. K. McGowan, P. H. Stelson, and W. G. Smith*

Oak Ridge National Laboratory, Oak Ridge, Tennessee

Thick-target yields have been measured for the Ni⁵⁸(α,γ) reaction from 4.9 to 6.1 MeV, the Ni⁵⁸(α,p) reaction from 4.9 to 11 MeV and the Co⁵⁹(α,n) reaction from 5.8 to 10 MeV. The reactions were identified by measuring the coincident annihilation radiation from the induced β⁺ activities. The absolute thick-target positron yields, which were measured at approximately 100-keV energy intervals, have an accuracy of ±6%. The reaction cross sections were obtained to an accuracy of 15 to 20% by the differentiation of the smooth thick-target yield curves. Over the measured energy range, the cross sections increase from 1 to 12 $\mu$b for the Ni⁵⁸(α,γ) reaction, 0.6 $\mu$b to 316 mb for the Ni⁵⁸(α,p) reaction, and 0.06 to 228 mb for the Co⁵⁹(α,n) reaction. The total reaction cross section for Ni⁵⁸ is compared to some values predicted by optical models. The Co⁵⁹(α,n) yields are compared to those obtained by measuring the neutrons directly with the graphite sphere detector.

## I. INTRODUCTION

FOR $\alpha$ particles with energies of 10 MeV or less, the total reaction cross section should be the sum of the following partial cross section; $(\alpha,n)$, $(\alpha,p)$, $(\alpha,\gamma)$, and $(\alpha,\alpha')$. The absolute $(\alpha,n)$ cross sections have been measured for a number of medium-weight targets.[1] The $(\alpha,n)$ threshold of 10.5 MeV for Ni⁵⁸ is unusually high. Furthermore, at 11 MeV the $(\alpha,n)$ cross section is only about 1/25 of those observed for the other nickel isotopes. Presumably, therefore, the bulk of the reaction cross section for $\alpha$ particles with energies of 11 MeV or less on Ni⁵⁸ must be attributed to the $(\alpha,p)$ reaction. Fortunately, the Ni⁵⁸(α,p)Cu⁶¹ reaction leads to a convenient radioactive nuclide. We have used the activation method to measure the Ni⁵⁸(α,p) cross section from $E_\alpha=4.9$ to 11 MeV.

The activation method has previously been used by Morinaga,[2] and by Ball, Fairhall, and Halpern[3] to measure the Ni⁵⁸(α,γ)Zn⁶² $\overset{\beta^+}{\rightarrow}$ Cu⁶² $\overset{\beta^+}{\rightarrow}$ Ni⁶² reaction. These measurements were made for $\alpha$-particle energies of about 10 MeV and higher. The observed cross sections were of the order of 100 $\mu$b. We have carried out measurements of the Ni⁵⁸(α,γ) cross section at the lower energies of 4.9 MeV$\leq E_\alpha \leq$6.1 MeV. At these energies the cross section varies from 1 to 10 $\mu$b. Good signal-to-noise conditions were attained by making a coincidence measurement of the annihilation $\gamma$ rays following the β⁺ decay.

* Deceased. Work conducted while on assignment to Oak Ridge National Laboratory as a summer research participant from Purdue University.

¹ P. H. Stelson and F. K. McGowan, following paper, Phys. Rev. 133, B911 (1964).

² H. Morinaga, Phys. Rev. 101, 100 (1956).

³ J. B. Ball, A. W. Fairhall, and I. Halpern, Phys. Rev. 114, 305 (1959).